Biosensors and Bioelectronics 128 (2019) 137–143

Contents lists available at ScienceDirect

Biosensors and Bioelectronics

journal homepage: www.elsevier.com/locate/bios

Photoelectrochemical biosensor for microRNA detection based on a MoS_2/g-C_3N_4/black TiO_2 heterojunction with Histostar@AuNPs for signal amplification

Minghui Wang[a], Huanshun Yin[a,*], Yunlei Zhou[a], Chengji Sui[a], Yue Wang[a], Xiangjian Meng[a], Geoffrey I.N. Waterhouse[a,b], Shiyun Ai[a,*]

[a] College of Chemistry and Material Science, Shandong Agricultural University, Taian 271018, PR China
[b] School of Chemical Sciences, The University of Auckland, Auckland 1142, New Zealand

ARTICLE INFO

Keywords:
Photoelectrochemical biosensor
MicroRNA detection
MoS_2/g-C_3N_4/black TiO_2 heterojunction
Histostar@AuNPs
S9.6 antibody

ABSTRACT

Herein, a novel photoelectrochemical (PEC) biosensor was developed for the ultrasensitive detection of microRNA-396a based on a MoS_2/g-C_3N_4/black TiO_2 heterojunction as the photoactive material and gold nanoparticles carrying Histostar antibodies (Histostar@AuNPs) for signal amplification. Briefly, MoS_2/g-C_3N_4/black TiO_2 was deposited on an indium tin oxide (ITO) electrode surface, after which gold nanoparticles (AuNPs) and probe DNA were assembled on the modified electrode. Hybridization with miRNA-396a resulted in a rigid DNA: RNA hybrid being formed, which was recognized by the S9.6 antibody. The captured antibody can further conjugate with the secondary IgG antibodies of Histostar@AuNPs, thereby leading to the immobilization of horse radish peroxidase (HRP). In the presence of HRP, the oxidation of 4-chloro-1-naphthol (4-CN) by H_2O_2 was accelerated, producing the insoluble product benzo-4-chlorohexadienone on the electrode surface and causing a significant decrease in the photocurrent. The developed biosensor could detect miRNA-396a at concentrations from 0.5 fM to 5000 fM, with a detection limit of 0.13 fM. Further, the proposed method can also be used to investigate the effect of heavy metal ions on the expression level of miRNAs. Results suggest that the biosensor developed herein offers a promising platform for the ultrasensitive detection of miRNA.

1. Introduction

MicroRNAs (miRNAs) are a class of endogenous and noncoding RNAs that play a crucial role in many biological processes in living organisms gene regulation, such as cell development, differentiation, metabolism, and apoptosis (Carthew and Sontheimer, 2009; Croce, 2009; Winter et al., 2009). MicroRNAs have a typical length of 18–25 nucleotides. Due to their high sequence homology, low content and ease-of-degradation, the detection of microRNAs is particularly challenging (Dong et al., 2013). Fast, reliable and sensitive methods for microRNA detection are needed. Various strategies have been explored for microRNA detection and quantification, including microarrays (Zhao et al., 2009), northern blotting (Pall et al., 2007), surface-enhanced Raman spectroscopy (SERS) (Driskell et al., 2008; He et al., 2017), electrochemiluminescence (Cheng et al., 2014; Feng et al., 2016; Wang et al. 2018c; Zhang et al., 2015), fluorescence (Dai et al., 2015; Dong et al., 2014; Miao et al., 2018), photoelectrochemical (PEC) (Hou et al., 2018; Ma et al., 2016; Wang et al. 2018b; Yin et al., 2014), and electrochemical methods (Hou et al., 2015; Wu et al., 2014; Zhou et al., 2016). Although miRNAs can be successfully detected using all of these techniques, PEC biosensors are especially attractive due to their low background noise, easy operation and excellent sensitivity. For PEC biosensors, appropriate choice of photoactive material(s) is critical to performance.

Recently, molybdenum disulfide (MoS_2) has received a lot of attention in the development of PEC biosensing platforms, due to its graphene-like structure, narrow band gap (1.2–1.9 eV), relatively high charge carrier mobility and high specific surface area (Wu et al., 2017). However, nonradiative electron-hole recombination in MoS_2 nanosheets limits the photoexcited carrier lifetimes to only few hundred picoseconds, which is highly detrimental to PEC sensor performance (Shi et al., 2013; Wang et al., 2015b). Accordingly, the discovery of effective strategies for charge separation, thereby increasing photoexcited carrier lifetimes, is vitally important to the successful integration of MoS_2 nanosheets in PEC biosensors.

The construction of the semiconductor heterojunctions is one of the

* Corresponding authors.
E-mail addresses: yinhs@sdau.edu.cn (H. Yin), ashy@sdau.edu.cn (S. Ai).

https://doi.org/10.1016/j.bios.2018.12.048
Received 15 October 2018; Received in revised form 12 December 2018; Accepted 21 December 2018
Available online 03 January 2019
0956-5663/

most efficient approaches for suppressing the recombination of photogenerated electrons and holes in semiconductor materials (Han et al., 2018; Liu et al., 2017). Potential gradients at semiconductors heterojunctions allow the facile migration of photoinduced charges (with electrons and holes typically migrating in opposite directions across the interface), thereby suppressing recombination and increasing photoexcited carrier lifetimes, resulting in enhanced PEC performance. The band edges of g-C_3N_4 are particularly well-matched with those of MoS_2 nanosheets (Li et al., 2016). For example, a PEC biosensor based on a MoS_2/g-C_3N_4 heterostructure was reported to display an excellent PEC performance, which was attributed to the abundance of surface active sites and increased charge separation (Wu et al., 2017). Ternary heterojunction structures involving three components can confer additional benefits due to their unique electronic and optical properties. Zhu's group reported a ultrasensitive PEC biosensor based on a ternary TiO_2/CdSeTe@CdS:Mn heterojunction (Fan et al., 2016). The ternary heterojunction benefitted from containing three distinct semiconductors, each with a different band gap, which combined synergistically to improve light absorption efficiency, promote electron transfer and extend the lifetime of charge carriers, thereby significantly increasing the PEC response.

Horseradish peroxidase (HRP) is an important heme-containing enzyme that has been studied for more than a century. The HRP-biocatalytic oxidation of 4-chloro-1-naphthol in the presence of H_2O_2, and forms insoluble products on the electrode, which can be used as an efficient amplification method for the sensing process (Alfonta et al., 2001). Histostar is a special immunohistochemical reagent based on many HRP labeled polymer conjugated with secondary antibodies (IgG). It can be used increase the availability of HRP at antigenic sites, thereby being very effective for signal amplification.

Herein, we report the successful development of a novel photoelectrochemical biosensor for microRNA detection based on a ternary MoS_2/g-C_3N_4/black TiO_2 heterojunction that used AuNPs conjugated with Histostar antibodies (Histostar@AuNPs) for signal amplification. This PEC biosensor exhibited high sensitivity and good specificity, reproducibility, and stability. The proposed strategy also provided a promising platform to help researchers clarify miRNA-396a regulatory networks and improve the rice tolerance to metal stress. There will be significant meaning for the regulation of heavy metal stress in different crops.

2. Experimental section

2.1. Detection strategy of the biosensor

Scheme 1A depicts the construction and operation of the PEC biosensor. Firstly, MoS_2, g-C_3N_4, b-TiO_2 and AuNPs were deposited on the bare ITO electrode surface, thereby forming a MoS_2/g-C_3N_4/black TiO_2 heterojunction as the photoelectric material (a detailed interpretation about the contribution of each material was described in Supplementary Material), with the AuNPs being used to immobilize probe DNA. Then the probe DNA was self-assembled on the electrode surface by the Au-S binding. In the presence of the miRNA-396a, a rigid DNA: RNA hybrid was formed, which could be recognized by S9.6

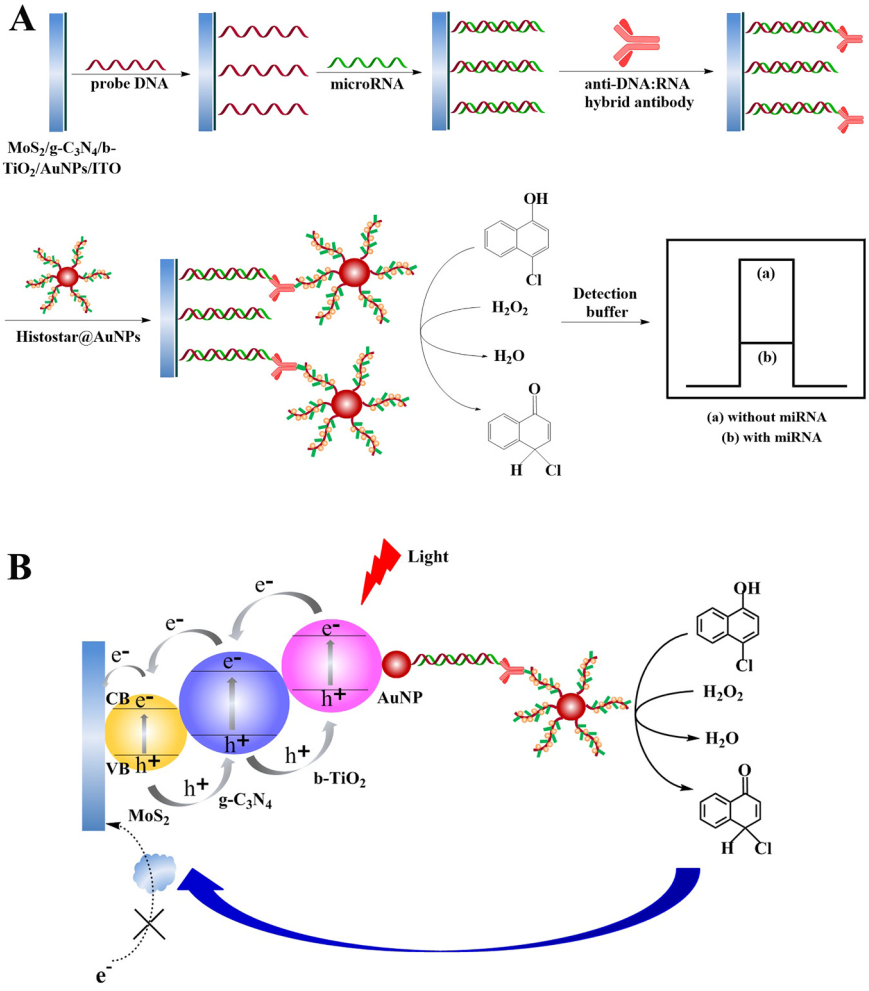

Scheme 1. Schematic illustration of the biosensor construction process (A) and the photocurrent generation mechanism of the PEC biosensor (B).

antibody due to the high specificity and affinity of the S9.6 antibody for DNA-RNA hybrids. After that, through the specific recognition effect between the primary antibody and the secondary antibody, the captured S9.6 antibody can further conjugate with the secondary antibody IgG in the composites of Histostar@AuNPs, leading to the immobilization of lots of HRP. As Histostar is a special immunohistochemical reagent based on many HRP labeled polymer conjugated with secondary antibodies (IgG), it can increase the availability of HRP at antigenic sites, leading to an effective amplification of the signal. In the presence of HRP, the oxidation of 4-chloro-1-naphthol (4-CN) by H_2O_2 was accelerated, producing the insoluble and insulating product benzo-4-chlorohexadienone on the electrode surface, causing a significant decrease in the photocurrent. From the linear relationship between the miRNA-396a concentration and the PEC response, sensitive detection of microRNA-396a can be achieved. To our knowledge, this work is the first to use black titania (b-TiO_2, E_g = 1.85 eV) in PEC sensor development, and builds on recent work aimed at the utilization of b-TiO_2 in the field of photocatalysis to increase solar spectrum utilization and enhance photocatalytic activities (Chen et al., 2011; Yan et al., 2017).

The photocurrent generation process of the biosensor, based on the MoS_2/g-C_3N_4/b-TiO_2 heterojunction, is depicted in Scheme 1B. MoS_2, g-C_3N_4 and b-TiO_2 possess band gaps of 1.8 eV, 2.72 eV and 1.85 eV, respectively which allowed the biosensor to make efficient use of incident visible light. Importantly, the valence band and conduction band edges of MoS_2, g-C_3N_4 and b-TiO_2 are staggered which allows rapid transfer of electrons and holes pairs between the semiconductors, thereby minimizing charge recombination and increasing the concentration of charge carriers. Hence, the photocurrent response of the biosensor was significantly enhanced through the introduction of the MoS_2/g-C_3N_4/b-TiO_2 heterojunction composite as the PEC platform.

2.2. Materials and apparatus

The materials and the buffers used in this work are provided in the Supplementary Materials.

Transmission electron microscopy (TEM) was performed on a Tecnai G2 F20 instrument (USA). Scanning electron microscopy (SEM) images were obtained using a Quanta Q400 (USA). Electrochemical impedance spectroscopy (EIS) data was collected on a CHI660C electrochemical workstation (CHI Instruments, Austin, TX). EIS data was collected in 10 mM Tris-HCl containing 5.0 mM $[Fe(CN)_6]^{3-/4-}$ solution and 0.1 M KCl (pH 7.4). PEC measurements were carried out on a CHI832A electrochemical workstation (Austin, USA) using a three-electrode system. A modified ITO electrode (0.195 cm^2) was used as the working electrode, a saturated calomel electrode (SCE) and a Pt wire were used as the reference electrode and the counter electrode, respectively. The photocurrent was recorded in PEC detection buffer under the visible light irradiation with an applied potential of 0.3 V. The irradiation source was supplied by a 500 W Xe lamp (Beijing Ceaulight Technology co., LTD., China).

2.3. Synthesis of MoS_2, g-C_3N_4, b-TiO_2 and AuNPs

MoS_2 was synthesized according to literature method (Ai et al., 2016). In brief, $(NH_4)_6Mo_7O_{24}{\cdot}4H_2O$ (4.3 mM) and thiourea (129 mM) were firstly dissolved in 150 mL of distilled water under vigorous stirring to form a homogeneous solution. Subsequently, the solution was transferred into a Teflon-lined autoclave (200 mL) and heated at 180 °C for 24 h. After cooling, the products were collected by centrifugation and washed three times with distilled water, and then dried under vacuum at 60 °C.

Graphitic carbon nitride (g-C_3N_4) was prepared from dicyanamide using a conventional thermal polymerization method (Wang et al. 2018b). Briefly, dicyandiamide (3.0 g) was placed in an alumina crucible with lid and then heated in air from room temperature to 220 °C at a heating rate of 3 °C min^{-1}, and then held at 220 °C for 2 h. The temperature was then increased to 350 °C (then held for 2 h) and finally 550 °C (held for 4 h). The product was then allowed to cool to room temperature naturally and washed with deionized water and ethanol several times. After drying in vacuum at 60 °C, the product was collected and ground into a powder for further use.

b-TiO_2 was synthesized according to previous report with a few modifications (Yan et al., 2016). TiO_2 (1 g) was firstly mixed with $NaBH_4$ powder (1 g) by grinding thoroughly with a mortar and pestle. After that, the mixture was transferred to an alumina boat and heated to 300 °C for 30 min under a N_2 atmosphere. The b-TiO_2 product was washed with water and ethanol, and dried under vacuum at 60 °C.

AuNPs were prepared according to a standard citrate reduction method (Liu and Lu, 2006). The Supplementary Materials contains details about the synthesis of the Au NPs and also a TEM image of the Au NPs (Fig. S1).

2.4. Preparation of Histostar@AuNPs (Hs@Au)

Histostar@AuNPs (denoted herein as Hs@Au) were prepared according to a literature method, with a few modifications (Wang et al., 2014). Firstly, the pH of the AuNPs dispersion (400 μL) was adjusted to 9.0 by addition of 0.1 M K_2CO_3. Then, Histostar (100 μL) was added to the AuNPs dispersion followed by continuous shaking for five min. After incubation at 4 °C for 12 h, 1 mL PEG 3350 (0.1%) was added and the resulting dispersion lightly shaken for 20 min. The dispersion was then centrifuged at 12,000 rpm for 30 min and the product washed with deionized water three times. Finally, the solid was redispersed in 1 mL of 10 mM PBS (pH 7.4) and stored at 4 °C.

2.5. Fabrication of the PEC biosensor

ITO conductive glass pieces (1 cm × 5 cm) were thoroughly cleaned according to our previous report (Li et al., 2017; Zhou et al., 2019). After cleaning, 40 μL of MoS_2, g-C_3N_4 and b-TiO_2 (each 2 mg/mL in water) were successively dropped onto the bare ITO electrode. After each semiconductor was added, the modified electrode was dried under an infrared lamp. The obtained electrode was denoted as b-TiO_2/g-C_3N_4/MoS_2/ITO. Then, 40 μL of the AuNPs dispersion was dropped on the electrode and the resulting electrode (Au/b-TiO_2/g-C_3N_4/MoS_2/ITO) dried under an infrared lamp. Subsequently, 40 μL of probe immobilization buffer containing 0.1 μM probe DNA was dropped on the Au/b-TiO_2/g-C_3N_4/MoS_2/ITO electrode surface and the electrode incubated for 4 h. The obtained electrode was denoted as p-DNA/Au/b-TiO_2/g-C_3N_4/MoS_2/ITO. After rinsing three times with washing buffer, 40 μL of miRNA hybridization buffer containing different concentrations of miRNA-396a were dropped onto the electrode and incubated for 2 h. The obtained electrode (RNA-DNA/Au/b-TiO_2/g-C_3N_4/MoS_2/ITO) was then rinsed three times with washing buffer. Next, the electrode was incubated with S9.6 antibody (40 μL, 20 μg/mL) for 1 h in a humid environment. The obtained electrode was denoted as Ab/RNA-DNA/Au/b-TiO_2/g-C_3N_4/MoS_2/ITO. After rinsing the electrode with washing buffer, 40 μL of Hs@Au was deposited on the electrode and incubated for 50 min, producing Hs@Au/Ab/RNA-DNA/Au/b-TiO_2/g-C_3N_4/MoS_2/ITO. Finally, the electrode was immersed in biocatalytic precipitation (BCP) solution containing 10 mM 4-CN and 0.15 mM H_2O_2. After incubated for 15 min, the electrode was rinsed with washing buffer and then used for PEC tests.

2.6. Sample preparation for the study of the effect of heavy metal ions on the expression level of micRNA-396a

Mature seeds of rice were used in this work. Firstly, rice seeds were embedded in gauze and soaked with deionized water for germination. Then, rice seedlings were treated with a solution containing Cd (II) ions to investigate the effect of heavy metal ions on the expression level of

microRNA-396a. In order to investigate the concentration effect, Cd (II) solutions of concentration 1, 10, 20, 50 or 100 mg/L were sprinkled on the leaves of rice seedlings as the water source and cultured for 24 h. For comparison, one group of rice seedling was cultured with distilled deionized water. Finally, the leaves were harvested for RNA extraction. The extraction was performed using a TRIzol® Plus RNA Purification Kit according to the manufacturer's recommended protocol (Invitrogen, USA).

3. Results and discussion

3.1. Characterization of materials

The morphologies of the MoS_2, g-C_3N_4 and b-TiO_2 materials used to fabricate the MoS_2/g-C_3N_4/black TiO_2 PEC heterojunction were characterized by TEM and the structural properties of b-TiO_2 were investigated by powder X-ray diffraction (XRD). The results were illustrated in Supplementary Materials (Fig. S2).

3.2. EIS Characterization of the biosensor

The stepwise fabrication process of the biosensor was followed by EIS and details were provided in Supplementary Materials (Figure. S3). The EIS experiments confirmed that each stage of biosensor fabrication was successful.

3.3. Detection feasibility assay

The detection feasibility of the biosensor was confirmed through PEC experiments. Fig. 1 shows that MoS_2/ITO (curve a), g-C_3N_4/ITO (curve b) and b-TiO_2/ITO (curve c) offered a weak photocurrent response under visible light irradiation. However, when g-C_3N_4 (curve d) and b-TiO_2 (curve e) were sequentially deposited on the MoS_2/ITO electrode, a significant increase in the photocurrent response were observed. The formation of the ternary semiconductor heterojunction was clearly beneficial for enhancing the photocurrent. Curve f and curve g show the PEC response after the final enzyme catalyzed BCP when the concentration of miRNA-396a was 0 fM and 5000 fM, respectively. Clearly, when the concentration of miRNA-396a was 5000 fM, the photocurrent decreased significantly due to the formation of insoluble benzo-4-chlorohexadienone on the electrode surface which acts as an insulating barrier on the electrode that hinders electron transfer. Results of Fig. 2 confirm that the proposed method is suitable for the detection of miRNA.

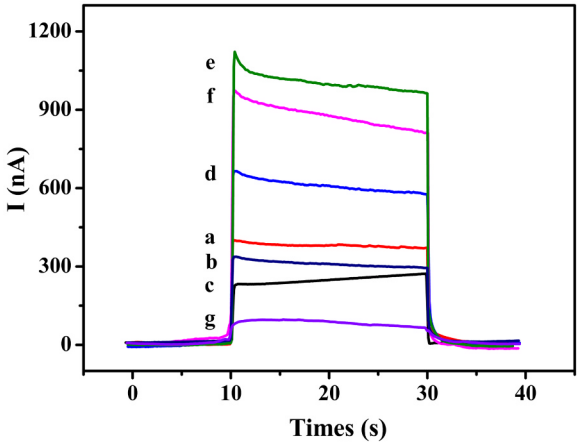

Fig. 1. The photocurrent response of (a) MoS_2/ITO, (b) g-C_3N_4/ITO, (c) b-TiO_2/ITO, (d) g-C_3N_4/MoS_2/ITO, (e) b-TiO_2/g-C_3N_4/MoS_2/ITO, (f) Hs@Au/Ab/RNA-DNA/Au/b-TiO_2/g-C_3N_4/MoS_2/ITO after a final enzyme catalyzed BCP when the miRNA-396a concentration was 0 fM, (g) Hs@Au/Ab/RNA-DNA/Au/b-TiO_2/g-C_3N_4/MoS_2/ITO after a final enzyme catalyzed BCP when the miRNA-396a concentration was 5000 fM.

3.4. Optimization of PEC biosensor testing conditions

To improve the efficiency and sensitivity of the biosensor, various experimental parameters needed to be optimized, including S9.6 concentration, S9.6 incubation time, Hs@Au immobilization time and biocatalytic precipitation (BCP) time. As shown in Fig. 2A, the PEC response decreased with S9.6 concentration in the range 0.1–20 μg mL^{-1}, which can be ascribed to the increased S9.6 increases the Hs@Au, resulting in the increase of HRP. Then the PEC response leveled off when the concentration was 20 μg mL^{-1} or higher due to the saturation of the S9.6 concentration.

Fig. 2B shows the effect of S9.6 incubation time on the PEC response of the biosensor. The photocurrent decreased with S9.6 incubation time up to 60 min, and then leveled off duo to the concentration of S9.6 had reached saturation. Accordingly, an incubation time of 60 min was used in all subsequent experiments.

Fig. 2C shows the effect of Hs@Au immobilization time on the PEC response of the biosensor. The photocurrent decreased with the incubation time from 10 to 50 min, then remained approximately constant at longer incubation times. It is due to the increase of time increases the Hs@Au, resulting in the increase of HRP, and the reaction will be saturated after a certain period of time. Thus, 50 min was selected as the optimal immobilization time. Finally, the BCP time was investigated (Fig. 2D). A time of around 15 min was identified as being near optimal and used in subsequent experiments.

3.5. Detection performance

Under the optimized experimental conditions, the ability of PEC biosensor to detect miRNA-396a was systematically investigated. As shown in Fig. 3A, the PEC response decreased with miRNA-396a concentration in the range 0.5 fM to 5 p.M. Fig. 3B reveals a strong linear relationship between the photocurrent and the logarithm of the miRNA-396a concentration. The regression equation was I (nA) = -19.43 log$c$ (fM) + 98.03, with a correlation coefficient (R) of 0.9948 and a low detection limit of 0.13 fM (S/N = 3). Compared with other methods for miRNA detection (Table 1), the PEC biosensor exhibited a wider linear range and also a relatively low detection limit, indicating its excellent performance.

To evaluate the selectivity of the proposed biosensor, miRNA-399c, miRNA-397b, miRNA-169b, miRNA-159c and single-base mismatched miRNA were chosen as possible interferants. As shown in Fig. 3C, the photocurrent response for miRNA-396a was significantly smaller than for the other miRNAs. Further, the PEC biosensor response to the miRNA-396a solution was near identical to the PEC biosensor response to a mixture containing miRNA-396a and the other miRNAs. The data confirms that the biosensor had a very good selectivity for miRNA-396a.

The reproducibility of the biosensor was also investigated. Six biosensors were fabricated independently using a microRNA-396a concentration of 50 fM (Fig. 3D). The relative standard deviation (RSD) value for the six biosensors was 2.4%, indicating that the biosensor had remarkable reproducibility.

The stability of the biosensor was also assessed. As shown in Fig. S4 (see Supplementary Materials), turning the light on and off 10 times within 400 s caused no obvious change in the detected photocurrent, confirming that the PEC signal was stable and reliable. In addition, a 2-week storage study was conducted to further investigate the stability of the biosensor. Following biosensor storage in a humid environment at 4 °C for 2 weeks, the measured photocurrent was ~ 92% of that

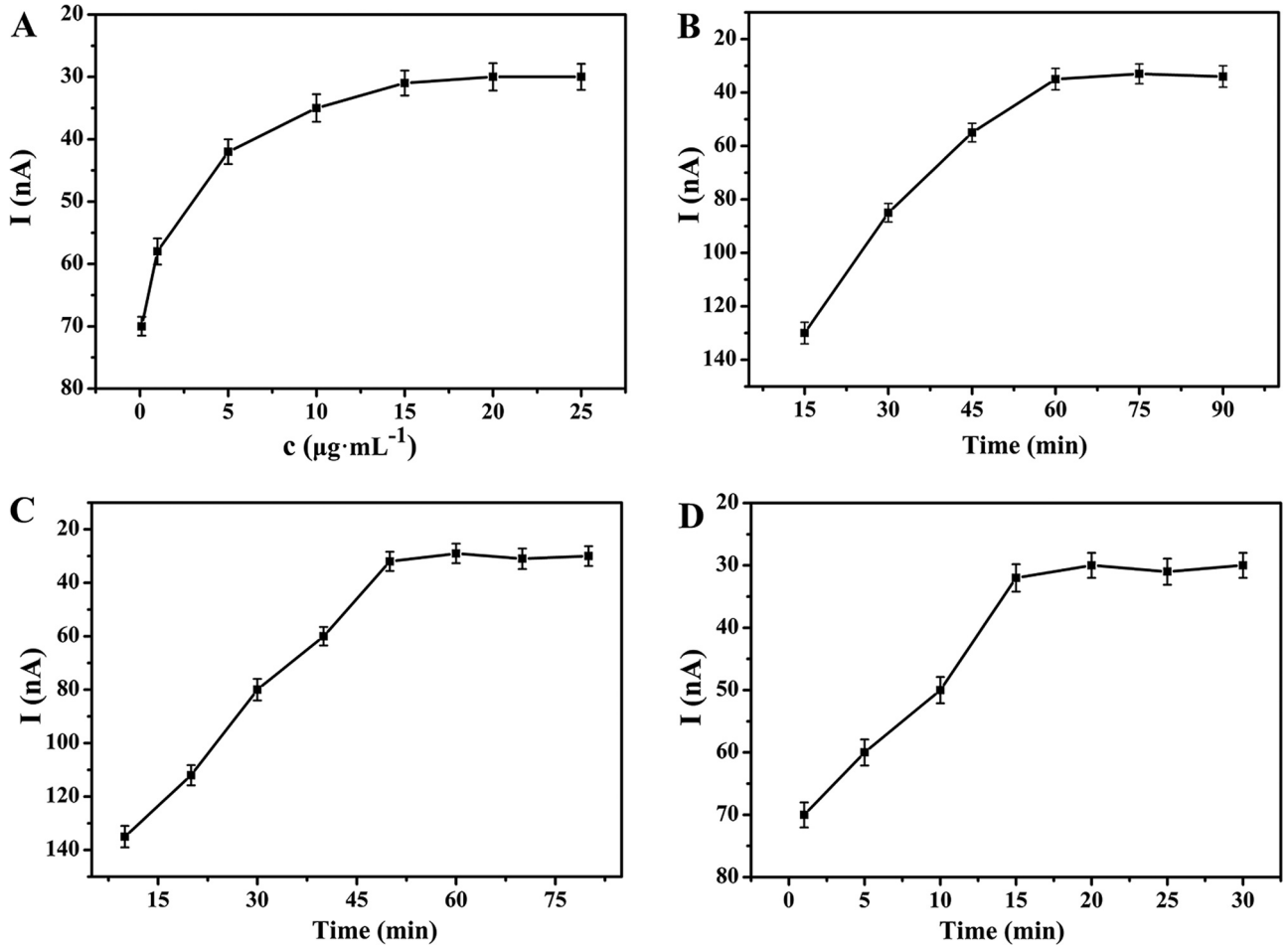

Fig. 2. Effects of S9.6 concentration (A), S9.6 incubation time (B), Hs@Au immobilization time (C), and BCP time (D) on the PEC response of the biosensor.

measured for the freshly prepared biosensor, demonstrating that biosensor showed very good stability.

3.6. Detection of miRNA-396a in real samples

To evaluate the analytical reliability and application potential, the proposed method was used to analysis miRNA-396a in total RNA extracted from leaves of rice seedlings. The total RNA was diluted to 200 ng μL^{-1} and used for detection. The amount of miRNA-396a in 200 ng of total RNA sample (blank control group treated with distilled deionized water) was estimated to be about 15 amol (75 fM in 200 μL of reaction buffer) (RSD = 1.2%, n = 5), according to the calibration curve (Fig. 3B). To evaluate its matrix effect, different amounts of miRNA-396a were spiked into 200 ng total RNA for the assay. The results showed the recovery of 108–111%, suggesting that the method have a low matrix effect, and great potential for sensitively detect miRNA in real sample (Table S2).

Heavy metal toxicity is a major factor that limit the growth and yield of crop plants, including rice. Cadmium (Cd) is considered to be one of the most harmful pollutants that cause serious toxicity to plants. Common symptoms of Cd injury include stunting, chlorosis, and even plant death (Rizwan et al., 2016). It is generally believed that an extensive understanding of plant miRNAs will significantly help induce tolerance against environmental stresses. The miRNAs and related gene characterization for Cd stress offer assistance in acknowledging the plant molecular mechanisms to heavy metal tolerance (Fang et al., 2013). Recent evidence suggests epigenetic mechanisms in regulating gene expression in plants under Cd stress, where the expression level of miRNA-396a normally decreased (Noman and Aqeel, 2017; Zhou et al., 2012).

In this work, the effect of heavy metal ions (Cd^{2+}) on the expression level of miRNA-396a in the leaves of rice seedlings was investigated. The total RNA of all samples was diluted to 200 ng μL^{-1} and used for detection. According to the calibration curve (Fig. 3B), the expression level of miRNA-396a in each sample was determined. The miRNA expression level of the blank control group was set to 1, and the relative expression levels of the other groups were 0.752, 0.375, 0.214, 0.176 and 0.121, respectively. As shown in Fig. 4, the expression level of microRNA-396a was down-regulated after treatment with Cd (II) ions, with the expression level decreasing with increasing Cd (II) concentration. The results reveal that Cd (II) ions affect the expression of miRNA and therefore may impair the growth and development of plants. To testing the accuracy of the proposed method, the expression level of miRNA-396a was also investigated by qRT-PCR. As shown in Fig. 4, the results obtained using qTR-PCR and our method were in excellent accord, verifying the accuracy of the biosensor. Employing this rapid and convenient method is able to help researchers clarify miRNA-396a regulatory networks and improve the rice tolerance to metal stress. There will be significant meaning for the regulation of heavy metal stress in different crops.

4. Conclusions

In summary, a novel PEC biosensor for ultrasensitive detection of miRNA was developed, based on MoS_2/g-C_3N_4/b-TiO_2 heterojunction as the photoactive platform and Histostar@AuNPs for signal

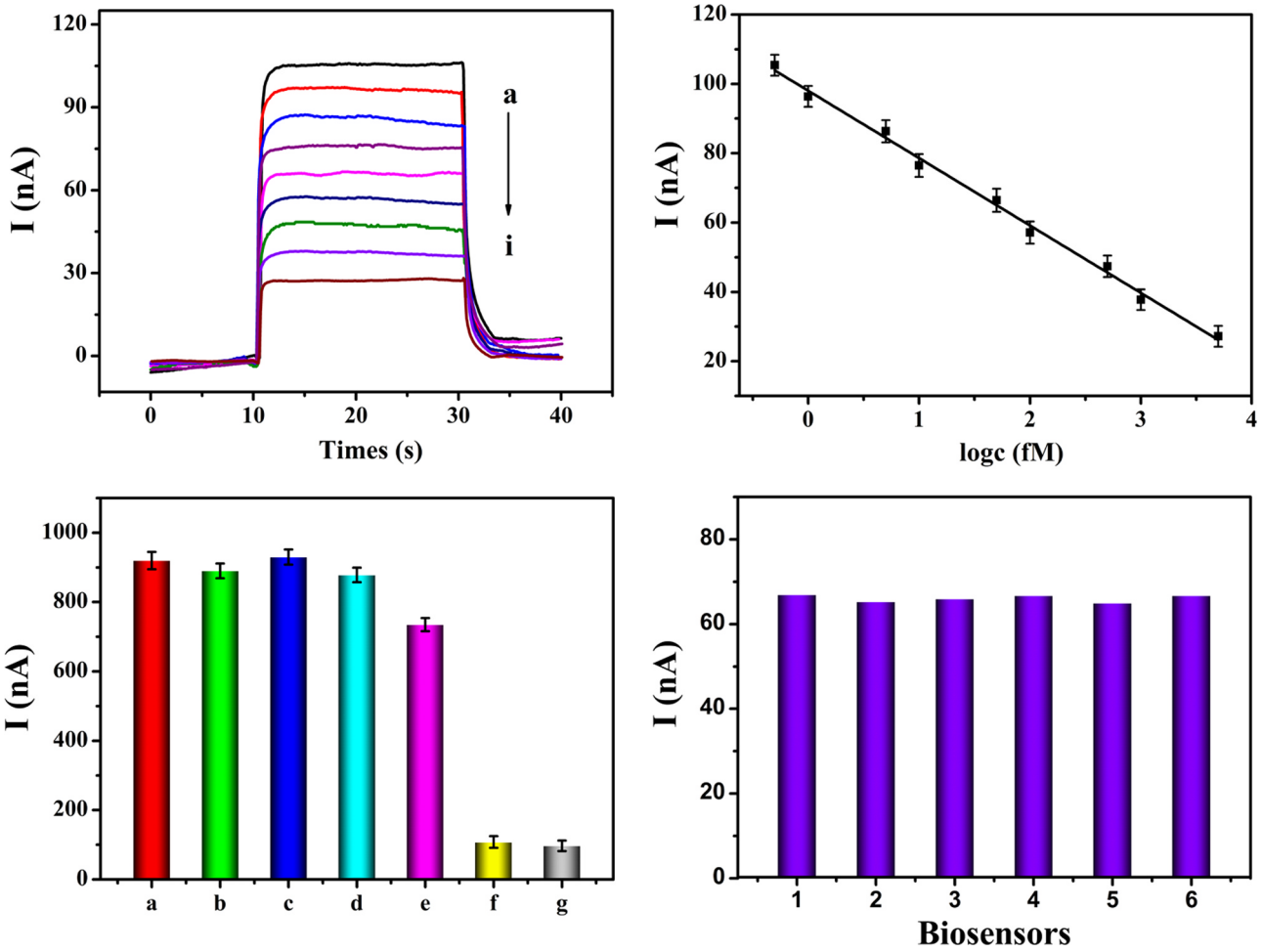

Fig. 3. (A) Photocurrent responses of the PEC biosensor at different concentrations of miRNA-396a. a-i, 0.5, 1, 5, 10, 50, 100, 500, 1000, 5000 fM. (B) Calibration curve of PEC response versus miRNA-396a concentration. Error bars represent the standard deviation of triplicate measurements. (C) Selectivity of the biosensor when analyzed with (a) miRNA-399c, (b) miRNA-397b, (c) miRNA-169b, (d) miRNA-159c, (e) single-base mismatched miRNA, (f) miRNA-396a, (g) mixture of miRNA-399c, miRNA-397b, miRNA-169b, miRNA-159c, single-base mismatched miRNA and miRNA-396a. (D) The reproducibility of the fabricated biosensor.

Table 1
Performance comparison of the PEC biosensor with other methods for miRNA detection.

Methods	Linear range	detection limit	reference
Electrochemistry	5–5000 fM	10 fM	(Koo et al., 2016)
Electrochemistry	1.0–1000 fM	0.434 fM	(Sun et al., 2018)
Fluorescence	0.01–200 nM	10 p.M.	(Wang et al., 2015a)
Fluorescence	0.1 nM to 8 μM	60 p.M.	(Lu et al., 2017)
ECL	1.0 fM to 1.0 nM	0.5 fM	(Feng et al., 2016)
ECL	50 fM to 100 nM	50 fM	(Lu et al., 2018)
PEC	5–3000 fM	2.26 fM	(Yin et al., 2016)
PEC	1.0 fM to 10.0 p.M.	0.5 fM	(Wang et al., 2018a)
PEC	0.5–5000 fM	0.13 fM	this work

amplification. To the best of our knowledge, this is the first time that b-TiO_2 and Histostar have been successfully applied in the field of biosensing. The biosensor offered a linear PEC response with miRNA-396a concentration in the range 0.5 fM to 5 p.M., with a low detection limit of 0.13 fM (S/N = 3). The high sensitivity for miRNA-396a can be attributed to the MoS_2/g-C_3N_4/b-TiO_2 heterojunction which increased charge carrier concentrations under light irradiation, and also the introduction of Histostar@AuNPs which enabled biocatalytic precipitation signal amplification. Results of this study suggest that the proposed biosensor offers a very promising low cost platform for the highly sensitive detection of miRNA.

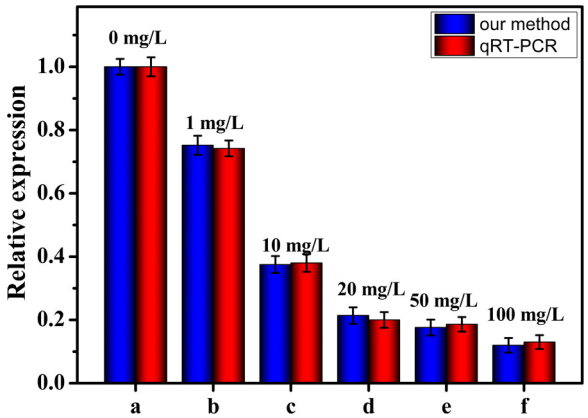

Fig. 4. Effect of different concentrations of Cd (II) ion (0, 1, 10, 20, 50 and 100 mg/L) on microRNA-396a expression.

Acknowledgements

This work was supported by the Natural Science Foundation of Shandong Province of China (No. ZR2014BQ029), the National Natural Science Foundation of China (No. 21775090, 21375079), Project of the Distinguished Young Scholar of Shandong Agricultural University, Founds of Shandong "Double Tops" Program (SYL2017XTTD15).

Declaration of interests

None.

Credit Author Statement

All the authors have been contributed for this work.

All the authors have been have made a significant contribution to the conception, design, execution, or interpretation of the reported study.

Appendix A. Supplementary material

Supplementary data associated with this article can be found in the online version at https://doi.org/10.1016/j.bios.2018.12.048.

References

Ai, K., Ruan, C., Shen, M., Lu, L., 2016. Adv. Funct. Mater. 26, 5542–5549.
Alfonta, L., Singh, A.K., Willner, I., 2001. Anal. Chem. 73, 91–102.
Carthew, R.W., Sontheimer, E.J., 2009. Cell 136, 642–655.
Chen, X., Liu, L., Yu, P.Y., Mao, S.S., 2011. Science1200448.
Cheng, Y., Lei, J., Chen, Y., Ju, H., 2014. Biosens. Bioelectron. 51, 431–436.
Croce, C.M., 2009. Nat. Rev. Genet. 10, 704.
Dai, W., Dong, H., Fugetsu, B., Cao, Y., Lu, H., Ma, X., Zhang, X., 2015. Small 11, 4158–4164.
Dong, H., Hao, K., Tian, Y., Jin, S., Lu, H., Zhou, S.-F., Zhang, X., 2014. Biosens. Bioelectron. 53, 377–383.
Dong, H., Lei, J., Ding, L., Wen, Y., Ju, H., Zhang, X., 2013. Chem. Rev. 113, 6207–6233.
Driskell, J.D., Seto, A.G., Jones, L.P., Jokela, S., Dluhy, R.A., Zhao, Y.P., Tripp, R.A., 2008. Biosens. Bioelectron. 24, 917–922.
Fan, G.-C., Zhu, H., Du, D., Zhang, J.-R., Zhu, J.-J., Lin, Y., 2016. Anal. Chem. 88, 3392–3399.
Fang, X., Zhao, Y., Ma, Q., Huang, Y., Wang, P., Zhang, J., Nian, H., Yang, C., 2013. Plos One 8, e81471.
Feng, Q.-M., Shen, Y.-Z., Li, M.-X., Zhang, Z.-L., Zhao, W., Xu, J.-J., Chen, H.-Y., 2016. Anal. Chem. 88, 937–944.
Han, Q., Wang, R., Xing, B., Chi, H., Wu, D., Wei, Q., 2018. Biosens. Bioelectron. 106, 7–13.
He, Y., Yang, X., Yuan, R., Chai, Y., 2017. Anal. Chem. 89, 8538–8544.
Hou, T., Li, W., Liu, X., Li, F., 2015. Anal. Chem. 87, 11368–11374.
Hou, T., Xu, N., Wang, W., Ge, L., Li, F., 2018. Anal. Chem. 90, 9591–9597.
Koo, K.M., Carrascosa, L.G., Shiddiky, M.J.A., Trau, M., 2016. Anal. Chem. 88, 2000–2005.
Li, J., Liu, E., Ma, Y., Hu, X., Wan, J., Sun, L., Fan, J., 2016. Appl. Surf. Sci. 364, 694–702.
Li, X., Zhu, L., Zhou, Y., Yin, H., Ai, S., 2017. Anal. Chem. 89, 2369–2376.
Liu, J., Lu, Y., 2006. Nat. Protoc. 1, 246.
Liu, Y., Shi, Y., Liu, X., Li, H., 2017. Appl. Surf. Sci. 396, 58–66.
Lu, L., Liu, C., Kang, T., Wang, X., Guo, G., Miao, W., 2018. Sens. Actuat. B-Chem. 255, 35–41.
Lu, S., Wang, S., Zhao, J., Sun, J., Yang, X., 2017. Anal. Chem. 89, 8429–8436.
Ma, Z.-Y., Xu, F., Qin, Y., Zhao, W.-W., Xu, J.-J., Chen, H.-Y., 2016. Anal. Chem. 88, 4183–4187.
Miao, X., Cheng, Z., Ma, H., Li, Z., Xue, N., Wang, P., 2018. Anal. Chem. 90, 1098–1103.
Noman, A., Aqeel, M., 2017. Environ. Sci. Pollut. R. 24, 10068–10082.
Pall, G.S., Codony-Servat, C., Byrne, J., Ritchie, L., Hamilton, A., 2007. Nucleic Acids Res. 35 (e60-e60).
Rizwan, M., Ali, S., Adrees, M., Rizvi, H., Zia-ur-Rehman, M., Hannan, F., Qayyum, M.F., Hafeez, F., Ok, Y.S., 2016. Environ. Sci. Pollut. R. 23, 17859–17879.
Shi, H., Yan, R., Bertolazzi, S., Brivio, J., Gao, B., Kis, A., Jena, D., Xing, H.G., Huang, L., 2013. ACS Nano 7, 1072–1080.
Sun, X., Wang, H., Jian, Y., Lan, F., Zhang, L., Liu, H., Ge, S., Yu, J., 2018. Biosens. Bioelectron. 105, 218–225.
Wang, B., Dong, Y.-X., Wang, Y.-L., Cao, J.-T., Ma, S.-H., Liu, Y.-M., 2018a. Sens. Actuat. B-Chem. 254, 159–165.
Wang, C., Zhang, H., Zeng, D., Sun, W., Zhang, H., Aldalbahi, A., Wang, Y., San, L., Fan, C., Zuo, X., Mi, X., 2015a. Nanoscale 7, 15822–15829.
Wang, H., Zhang, C., Rana, F., 2015b. Nano Lett. 15, 8204–8210.
Wang, M., Yin, H., Shen, N., Xu, Z., Sun, B., Ai, S., 2014. Biosens. Bioelectron. 53, 232–237.
Wang, M., Yin, H., Zhou, Y., Han, J., He, T., Cui, L., Ai, S., 2018a. Microchim. Acta 185, 257.
Wang, M., Zhou, Y., Yin, H., Jiang, W., Wang, H., Ai, S., 2018b. Biosens. Bioelectron. 107, 34–39.
Winter, J., Jung, S., Keller, S., Gregory, R.I., Diederichs, S., 2009. Nat. Cell Biol. 11, 228.
Wu, S., Huang, H., Shang, M., Du, C., Wu, Y., Song, W., 2017. Biosens. Bioelectron. 92, 646–653.
Wu, X., Chai, Y., Yuan, R., Zhuo, Y., Chen, Y., 2014. Sens. Actuat. B-Chem. 203, 296–302.
Yan, B., Zhou, P., Xu, Q., Zhou, X., Xu, D., Zhu, J., 2016. RSC Adv. 6, 6133–6137.
Yan, X., Xing, Z., Cao, Y., Hu, M., Li, Z., Wu, X., Zhu, Q., Yang, S., Zhou, W., 2017. Appl. Catal. B: Environ. 219, 572–579.
Yin, H., Wang, M., Zhou, Y., Zhang, X., Sun, B., Wang, G., Ai, S., 2014. Biosens. Bioelectron. 53, 175–181.
Yin, H., Zhou, Y., Li, B., Li, X., Yang, Z., Ai, S., Zhang, X., 2016. Sens. Actuat. B-Chem. 222, 1119–1126.
Zhang, P., Wu, X., Yuan, R., Chai, Y., 2015. Anal. Chem. 87, 3202–3207.
Zhao, J.-J., Yang, J., Lin, J., Yao, N., Zhu, Y., Zheng, J., Xu, J., Cheng, J.Q., Lin, J.-Y., Ma, X., 2009. Child'S. Nerv. Syst. 25, 13–20.
Zhou, Y., Yin, H., Li, J., Li, B., Li, X., Ai, S., Zhang, X., 2016. Biosens. Bioelectron. 79, 79–85.
Zhou, Y., Yin, H., Sui, C., Wang, Y., Ai, S., 2019. Chem. Eng. J. 357, 94–102.
Zhou, Z.S., Song, J.B., Yang, Z.M., 2012. J. Exp. Bot. 63, 4597–4613.